Biomedical Signal Processing and Control 18 (2015) 110–117

Contents lists available at ScienceDirect

Biomedical Signal Processing and Control

journal homepage: www.elsevier.com/locate/bspc

Volume visualization based on the intensity and SUSAN transfer function spaces

Yipeng Song [a], Jie Yang [a,*], Yu Qiao [a], Yuemin Zhu [b]

[a] Institute of Image Processing and Pattern recognition, Shanghai Jiao Tong University, Shanghai 200240, China
[b] CREATIS, CNRS UMR 5220, Inserm U1044, INSA Lyon, University of Lyon, Villeurbanne 69100, France

ARTICLE INFO

Article history:
Received 22 July 2014
Received in revised form
18 November 2014
Accepted 5 December 2014
Available online 3 January 2015

Keywords:
Direct volume rendering
Transfer function
3D SUSAN algorithm
Volume visualization

ABSTRACT

Designing transfer functions is a challenging task for medical volume data visualization, especially when an arch of the same boundary disperses seriously and adjacent arches are intersected in the intensity and gradient magnitude (IGM) transfer function space. In this paper, a novel transfer function space is proposed to better highlight and differentiate different materials in realistic volume datasets. The proposed method combines the intensity values and three-dimensional (3D) SUSAN (Smallest Univalue Segment Assimilating Nucleus) edge responses of the original data to define the intensity and SUSAN (IS) transfer function space. The results of various datasets in volume rendering show that boundary of different materials exhibits a trapezoidal shape in the proposed IS space, and boundary information is much better brought out in comparison to the IGM space. Thus the IS space provides much more intuitive clues than the IGM space in order that transfer functions can be more easily designed. Meanwhile, more details of materials of interest are visible in the rendering images.

1. Introduction

With many state-of-the-art imaging modalities used in medicine (e.g., computed tomography (CT) and magnetic resonance imaging (MRI)), a great number of medical volume datasets are being obtained (Fig. 1(a)). Thus there is an urgent need to provide useful methods for identifying structures of interest and obtaining meaningful visualizations of anatomical structures (Fig. 1(b)). A variety of algorithms have been proposed to identify and segment anatomical structures in different volume datasets [1,2] and some rendering techniques are used to render segmented structures [3–5].

Direct volume rendering has been proven to be a more useful technique to explore and visualize structures of interest and reveal hidden interesting organs in medical volume data [6,7]. Users can not only easily understand boundary information from the transfer function spaces, but also intuitively design transfer functions while observe 3D visualizations according to adjusted transfer functions (Fig. 1(c)). Therefore, transfer function is a critical element in direct volume rendering. By designing different transfer functions which assign optical properties (e.g., color and opacity) to each voxel, different anatomical structures in volume data can be visualized and distinguished by ray casting algorithms [5,8]. In most cases, no prior information can be available in the volume data, which makes feature selection in the transfer function space become a trial-and-error process. Consequently, an effective transfer function space which can help users to easily distinguish and identify useful features, is necessary and beneficial to get desirable renderings.

The transfer function space is defined by using the intensity value or other attributes of the original volume data. As one-dimensional transfer function space [5,9] solely uses intensity values to enhance structures of interest, all voxels having the same intensity values are rendered by the same optical properties which are assigned by transfer functions, no matter whether they belong to the same structure. To discriminate those voxels, multi-dimensional transfer function spaces have been proposed, which use additional properties. In particular, two-dimensional (2D) IGM transfer function space (as shown in Fig. 2(b)) has been proposed to discern features of interest and extract material boundaries [6,10]. In this approach, boundaries of different materials having large gradient values are shown as arches in the space and they are different from homogeneous regions having small gradient values in the space (Figs. 4(b) and 11(f)). Therefore, boundaries of structures of interest can be enhanced by using transfer functions to assign bigger opaque values than interior voxels. Even users can set the opaque values of those interior voxels to zero to eliminate

* Corresponding author. Tel.: +86 21 34204033.
E-mail address: jieyang@sjtu.edu.cn (J. Yang).

http://dx.doi.org/10.1016/j.bspc.2014.12.002
1746-8094/

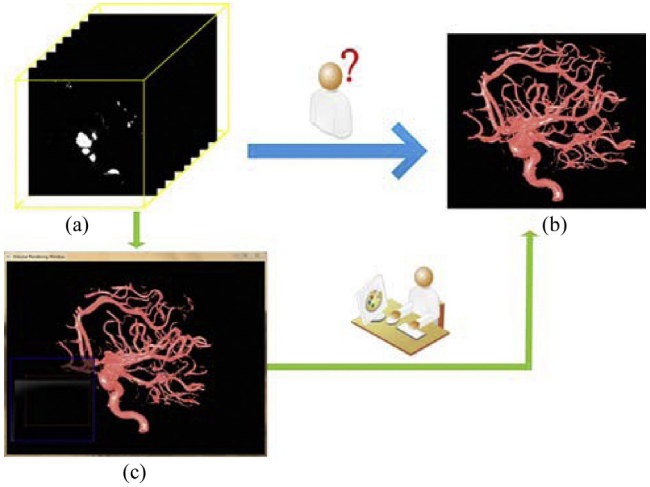

Fig. 1. The meaningful image (b) of an aneurysm volume data (a) is obtained by using direct volume rendering (c).

the influence of these undesirable tissues. By utilizing interaction manipulation widgets to select arch shapes [6] (as shown in Figs. 3(c) and 10(d)), transfer functions can be designed by users and used to assign different optical properties to different anatomical structures (Figs. 3(d) and 10(b)). Unfortunately, for realistic volume data, dispersed arches of the same boundary (Figs. 10(d) and 11), incomplete arch of different materials (Figs. 2(b) and 8(a)) and lost arch information (Fig. 4(b)) often occur in the IGM space. As a result, it is difficult for users to design appropriate transfer functions and distinguish structures of interest.

Chen et al. [11] tried to use information theory to explain many existing visualization techniques and use it as a theoretic framework for visualization. Roettger et al. [12] added spatial information into the IGM space by deriving the color for easier classification. Wang et al. [13] modeled the IGM space using the Gaussian mixture model to automatically separate initial features. Marks et al. [14] simplified the transfer function's design process by selecting the most proper rendering results from design galleries. Maciejewski [7] defined abstract feature space with a set of metrics derived from the spatial and feature space domains. Park and Bajaj [15] introduced stretched histogram to distinguish overlapping features. Serlie et al. [16] introduced an arch edge model and modeled the neighborhood of sample points by an arch trajectory which makes the technique against erroneous classification resulting from noise. Correa and Ma [17] described feature size using the relative size of each voxel and mapped it to optical parameters. Wesarg et al. [18] derived the size of anatomical structures from volume data by

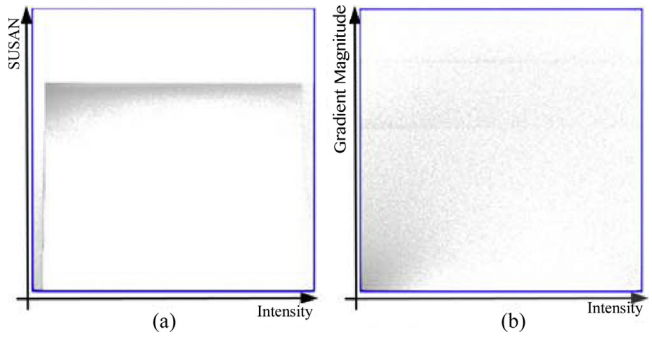

Fig. 2. Comparing explorations of an aneurysm data set using an IS space (a) and IGM space (b). Here, the brightness of the 2D bins represents its frequency used in the logarithmic scale [6]. (To more clearly, the two spaces are shown by reversed.)

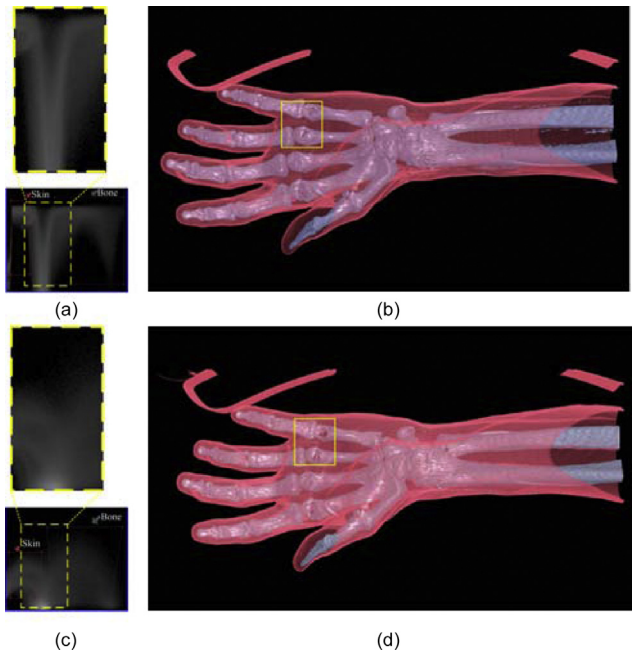

Fig. 3. (b) Visualizations of a CT hand data by using the settings of the IS space in (a) are compared with (d) ones by using the IGM space (c). The proposed space (yellow window in (a)) can significantly reduces overlapping regions of bone and skin in the IGM space (yellow window in (c)) and obtain intuitive 'trapezoid' shapes. (For interpretation of the references to color in this figure legend, the reader is referred to the web version of the article.)

using a threshold-based voxel counting technique and used it as a second property.

Marchesin et al. [19] presented the per-pixel-modulated rendering to enhance feature visibility. Wu and Qu [20] proposed a framework for editing resulting images, in which users could directly edit features in rendering images and interactively design transfer functions. Chan et al. [21] rendered images by optimizing the rendering parameters based on visibility, shape, and transparency measures to comply with users' perception. Ruiz et al. [22] presented an approach to automatically design transfer function.

How to visualize more internal structures is one of the most important problems in direct volume rendering. Visibility-based transfer function space was introduced by Correa and Ma [23] to maximize the visibility of interesting features. By using LIDA accumulation [24], more details of the volume data are rendered.

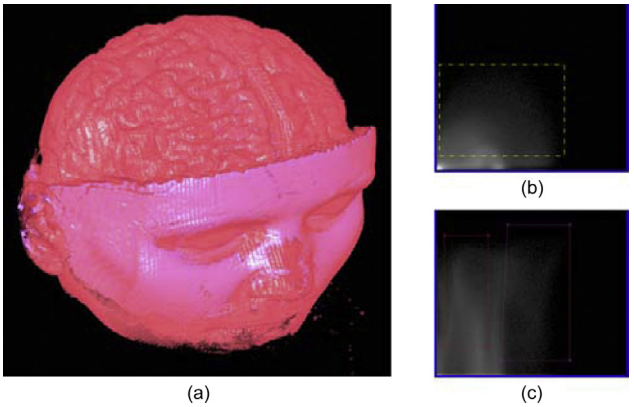

Fig. 4. Comparing explorations of a MR head data using a traditional 2D IGM space (b) and the 2D IS space (c). (a) Rending results obtained with the IS space (c). (For interpretation of the references to color in this figure legend, the reader is referred to the web version of the article.)

Correa and Ma [25] introduced an occlusion spectrum to separate structures in volume data, which encodes the 2D distribution of intensity values and occlusion. Viola et al. [26] introduced the importance-driven feature enhancement approach for automatic focus + context volume rendering. Praßni et al. [27] presented a novel shape-based classification technique for volume visualization by which users distinguished features based on 3D shape and assigned different optical properties to them.

Smith and Brady [28] used a completely new definition of edges and proposed the SUSAN algorithm. Owing to its property of structure preserving and noise reduction, the algorithm has been applied to various image vision problems. Marusic et al. [29] applied the SUSAN algorithm to reduce coding artifacts in wavelet video-coding. Mao et al. [30] extended the SUSAN operator to denoise 3D meshes. Claus et al. [31] optimized the SUSAN algorithm by a high speed FPGA implementation. Yu et al. [32] introduced the SUSAN detectors to guide diffusion process, and created the SUSAN-controlled anisotropic diffusion model for speckle reduction and detail preservation.

Partial-volume effect (PVE) resulting from the mixture of intensities of voxels belonging to different regions can make boundaries become blurred and exacerbate the ability to recognize 'arch' shapes in the IGM space (the x axis represents intensity, the y axis gradient magnitude) (see Fig. 2(b)). The presence of noise in volume data is a typical phenomenon in realistic circumstances, which results in variations of the intensity values around an average value and multiple arches for the same boundary in the IGM transfer function space as shown in Fig. 10(d). Therefore, it is difficult to discern boundary information of interesting structures in the IGM space, especially when different arches are intersected (yellow window in Fig. 3(c)). As a result, anatomical structures of interest cannot be easily explored and visualized just using the 2D IGM transfer function space.

Therefore, in this paper, we address these problems by introducing a new IS transfer function space. By combining intensity value of the original data and 3D SUSAN edge responses of each voxel, the IS transfer function space is created, in which boundaries of different materials represent 'trapezoid' shapes and boundary information is much better brought out (Figs. 2(a) and 10(c)). Thus the IS space provides much more intuitive suggestions than the IGM space and transfer functions can be more easily designed. Also, we can obtained more details of materials of interest (Figs. 3(b), 8(c) and 11(c)).

2. Methods

As shown in the IGM space of Figs. 2(b) and 10(d), 'arch' shapes of the same boundary are disperses seriously in order that users cannot intuitively recognize arch information to design transfer functions and visualize anatomical structures of interest. When adjacent arches belonging to different boundary are intersected (Fig. 3(c)) and there are not incomplete 'arch' shapes (Fig. 8(a)), it is difficult for users to understand the IGM space and set appropriate transfer functions. Even different 'arch' shapes could overlap in the IGM space, which makes it impossible for users to distinguish these arch information (Fig. 4(b)). To deal with these problems, we introduce the IS transfer function space, in which boundaries of different materials represent 'trapezoid' shapes and boundary information is much better brought out. With the IS space, we can obtain much more intuitive suggestions for understanding the transfer function space and easily design transfer functions.

The overview of the proposed transfer function method is presented in Fig. 5. To get images rendering from the IS transfer functions, several processing steps are required. Firstly, the properties of IS space (i.e., intensity and SUSAN responses) are extracted.

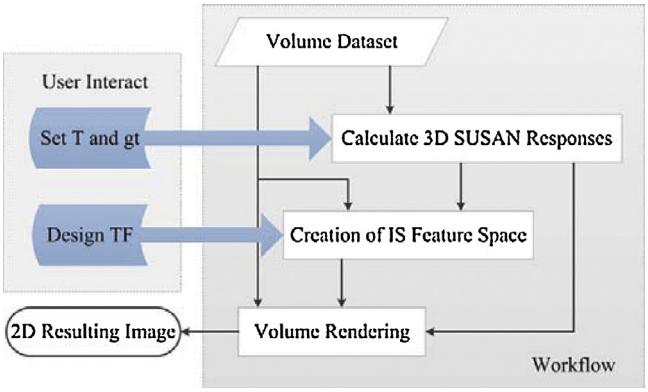

Fig. 5. The workflow of the IS transfer function.

The number of the voxels having the same property values in the volume data are counted for each pixel in the IS space and then the space is constructed. To visualize anatomical structures, the transfer function space can provide clues for users to design meaningful transfer functions. Finally, resulting images are rendered with ray casting algorithm [5,8] by using optical properties from designed transfer functions.

2.1. Computation of 3D SUSAN responses

Since 3D SUSAN allows us to reduce noise and preserve detail information, we use it as a second property to define a new 2D transfer function space. In medical volume data, such as MRI or CT data, the intensity value of voxels may be altered around a certain value due to noise and PVE, which leads to the IGM space difficult to understand (see Figs. 2(b), 4(b) and 10(d)) and transfer functions difficult to correctly design. In this paper, we define the IS space by using intensity value and 3D SUSAN edge responses to deal with these problems. In the following section, we explain the spherical neighborhood and the principle of 3D SUSAN algorithm.

2.1.1. The spherical neighborhood

The 3D SUSAN algorithm employs a spherical mask centered on each voxel of the volume data and applies a local threshold based rule on intensity values so as to achieve isotropic response that results in the output of the edge responses. Therefore, when counting the number of voxels in the spherical neighborhood having the similar intensity value assigned to the center voxel, we need to traverse the entire region until the similarity condition is fulfilled. While the spherical mask is calculated by numerical approximations with constant weighting in a neighborhood of predetermined size. To balance mask of traditional SUSAN algorithm [28] and complexity of 3D volume data, the usual size of radius is set as 4.0 voxels, which gives a mask of 251 voxels (see the 3D green regions shown in Fig. 6(a)) and gives isotropic responses. The spherical neighborhood of 251 voxels is used in all volume experiments unless otherwise indicated.

2.1.2. The principle of 3D SUSAN algorithm

The SUSAN algorithm was initially introduced by Smith et al. [28]. The basic principle of SUSAN algorithm is to associate each pixel of the image with the number of neighbor pixels having similar intensity to this (center) pixel. The number of pixels is called the Univalue Segment Assimilating Nucleus (USAN), which contains important structure information in the region around the center pixel.

The 3D SUSAN responses consist in laying the spherical mask at each voxel in the volume data, and comparing the intensity of

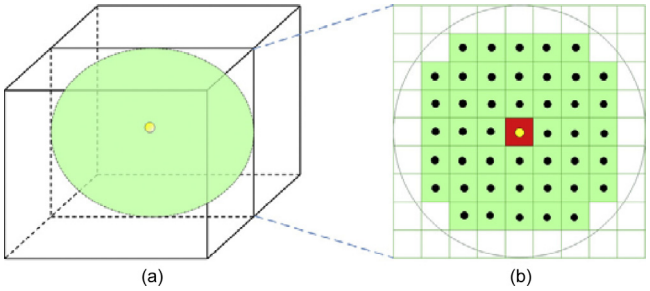

Fig. 6. (a) The spherical neighborhood of a center voxel (yellow) and (b) its 2D slice with the voxels in black. (For interpretation of the references to color in this figure legend, the reader is referred to the web version of the article.)

each voxel in the neighborhood with that of the nucleus (the center voxel). The comparison is performed using:

$$c\_bool(\vec{r}_j, \vec{r}_i) = \begin{cases} 1 & \text{if } |I(\vec{r}_j) - I(\vec{r}_i)| \le T \\ 0 & \text{if } |I(\vec{r}_j) - I(\vec{r}_i)| > T \end{cases} \quad (1)$$

where $I(\vec{r}_i)$ is the intensity of the nucleus located at $\vec{r}_i = (r_{ix}, r_{iy}, r_{iz})$ in volume data, $I(\vec{r}_j)$ is the intensity of any other voxel $\vec{r}_j$ within the mask, T is the intensity difference threshold relative to the minimum contrast of features to be detected and the maximum amount of noise to be ignored, and *c_bool* is the output of the comparison. If the comparison is smaller than T, the output is equal to one, otherwise it is zero.

The comparison is performed for each voxel within the spherical mask, so the total of the outputs, which constitutes the USAN's area, is counted:

$$num(\vec{r}_i) = \sum_{|\vec{r}_j - \vec{r}_i| < \delta} c\_bool(\vec{r}_j, \vec{r}_i) \quad (2)$$

where $|\vec{r}_j - \vec{r}_i| = \sqrt{(r_{jx} - r_{ix})^2 + (r_{jy} - r_{iy})^2 + (r_{jz} - r_{iz})^2}$ is the distance between the voxel located at $\vec{r}_j$ and the nucleus at $\vec{r}_i$, and δ is the radius of the spherical neighborhood.

Therefore, the USAN area is maximum when the center voxel is inside a relatively homogeneous region, while it turns to half of this maximum near a straight boundary and falls even further when inside sharp regions. It is the main property of the USAN's area and used as the detector of edges. So, the smaller the USAN, the larger the edge response. The edge response is described by

$$er(\vec{r}_i) = \begin{cases} gt - num(\vec{r}_i) & \text{if } num(\vec{r}_i) \le gt \\ 0 & \text{otherwise} \end{cases} \quad (3)$$

where *gt* is a geometric threshold calculated as

$$gt = k \times num_{\max} \quad (4)$$

and $num_{\max}$ is the maximum value that *num* can take. Generally, k is set to 3/4 in order to give optimal noise rejection, and the value is obtained by analyzing the expectation value of the response in the presence of noise. The circumstantial derivation process may refer to [28]. According to the volume data in question, k can be adjusted to achieve a better classification effect and avoid incorrect dismissal of correct edges. Non-maximum suppression was implemented, and the edge enhancement was then completed.

In our method, we apply a more stable and sensible equation proposed by Smith et al. [28] to calculate comparison function in place of Eq. (1):

$$c\_stable(\vec{r}_j, \vec{r}_i) = \exp\left(-\left(\frac{I(\vec{r}_j) - I(\vec{r}_i)}{T}\right)^6\right) \quad (5)$$

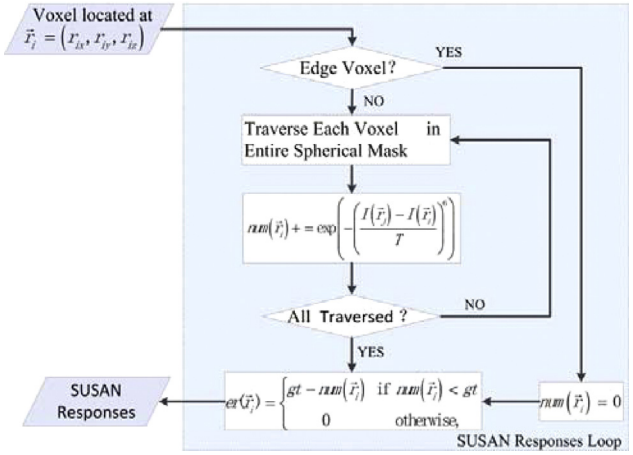

Fig. 7. Calculation of 3D SUSAN responses.

This can reduce the large effect on the comparison function when a voxel's intensity varies slightly, even if it is near the threshold T.

Therefore, for each voxel in the volume data, the SUSAN responses can be directly calculated. First, we need to determine whether the voxel is around the edge of volume data. If it is, due to its intensity value is almost zero and cannot affect the IS space, the number of USAN's area is equal to zero. Otherwise, we will traverse each voxel inside the whole spherical neighborhood of the nucleus using Eq. (5) to compute intensity similarity between it and the center voxel. Then, we count the number of voxels in the USAN's area using Eq. (2). Finally we utilize Eq. (3) to calculate the 3D SUSAN responses. The flowchart of computing the SUSAN responses of one voxel is illustrated in Fig. 7.

2.2. Creation of the IS space

The IS transfer function space is created by using intensity as the first property and the 3D SUSAN edge response as the second property (Fig. 2(a)). The IS space is constructed as follows:

1. Set ranges on the 2D transfer function space axes from 0 to 255 and initialize the bins of the space to all zeros.
2. Traverse through the entire volume data. Compute $er(\vec{r}_i)$ of each voxel using Eq. (3). In the present study, we set $T = 20$ for MR volume datasets which are contaminated seriously by noise and $T = 10$ for CT. $k = 3/4$. These values work in most cases. Meanwhile, search for the highest value and the lowest value of the response.
3. During the second traverse, modulate the range of *er* into [0, 255], then accumulate the number of voxels with the same [*I*,*er*] coordinates to build an IS transfer function space, in which the intensity value shows the mount of contributions: black is lowest, white highest, and the amount of contributions is shown in logarithmic scale [6] (see Figs. 3(a) and 9(c)).

Faced with transfer function window (as the blue window shown in Fig. 1(c)), users design a transfer function by using a process of exploration and refinement. Initially, users added a classification widget to the transfer function window according to 'trapezoid' shapes in the blue window (bottom-left in Fig. 1(c)), and a rendering image using the transfer function is presented that may bring out some structures of interest (the aneurysm is shown in Fig. 1(c)). Each widget has some control points and lines that users can modify their positions, sizes or optical properties (e.g., opacity and color) (red quadrilateral widget in Fig. 1(c)). The color and opacity values from each widget are blended together to

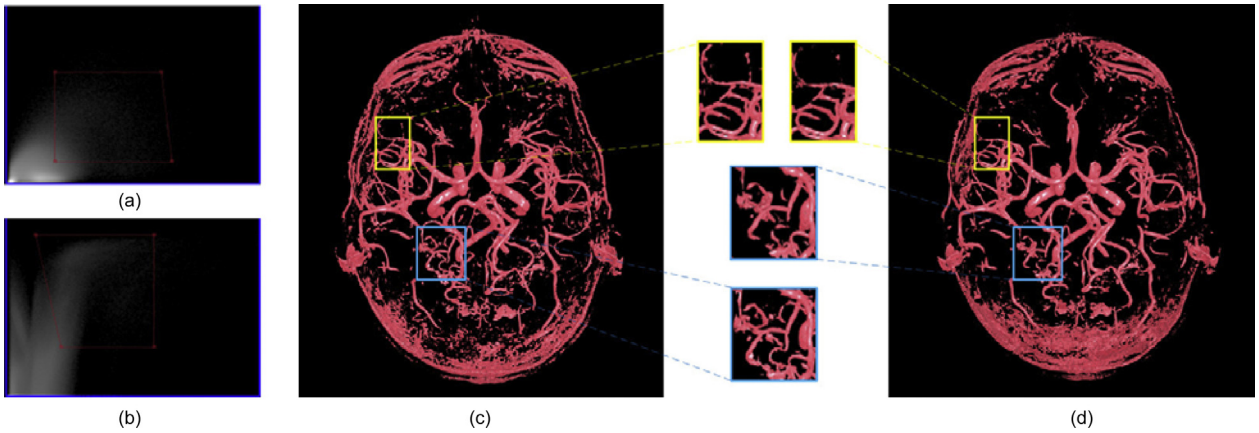

Fig. 8. Comparison of the IS space (b) with the IGM space (a) on identifying arteries. (c) The image is rendered by the IS space (b). (d) The resulting image by the IGM space (a). The proposed method can get more complete fine veins (yellow window) and more tiny vessels (blue window). (For interpretation of the references to color in this figure legend, the reader is referred to the web version of the article.)

constitute transfer functions and the rendering results are generated by these renderable properties [5,6,8]. Users can modify the classification widgets while continually updating the rendering result. Once the region in the transfer function space have been distinguished, users can refine it by manipulating control points of the widget to better visualize structures.

From the described process, it is clear that the transfer function space plays a very important role in direct volume rendering. From experiments of variously realistic volume data, it turns out that the IS space is more intuitive for users to obtain useful suggestions of boundary information and easily design transfer functions than the IGM space. Firstly, unlike 'arch' shapes of the same boundary are disperses seriously in the IGM space (Figs. 2(b) and 10(d)), 'trapezoid' shapes in the proposed space are more compact and centralized (Figs. 2(a) and 10(c)). It is more intuitive for users to design transfer functions just by setting simple rectangular windows to enwrap the salient regions and obtain desired results. Secondly, the IS space can obtain more complete boundary information of different materials than the IGM space (as shown in Fig. 8), even if adjacent arches of different boundary are intersected in the IGM space (Fig. 3(c)). It is much more intuitive for users to understand the boundary information in the transfer function space. Finally, when different 'arch' shapes overlap in the IGM space and they almost form a single arch (Fig. 4(b)), it is impossible for users to distinguish these arches in the IGM space. While the proposed space can not only significantly reduces overlapping regions in the IGM space, but also makes these arches more easily identify (Fig. 4(c)). To illustrate its intuitive, an informal user opinion survey about three representative volume data (Figs. 2–4) is done for six novice transfer function designers in the next section.

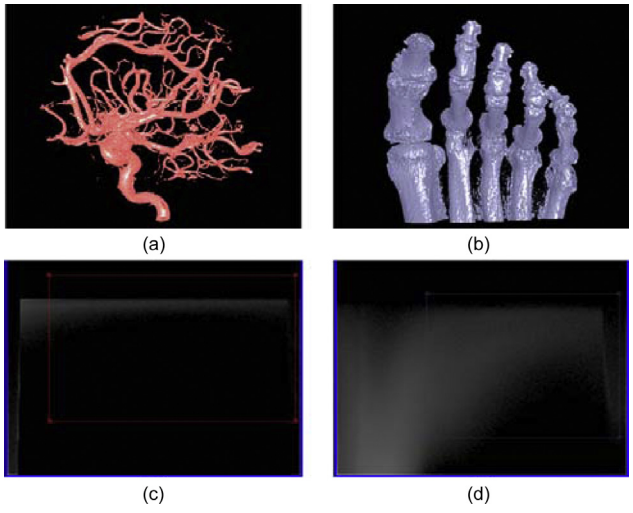

Fig. 9. (a) The result of the aneurysm data (Fig. 1) used in Fig. 2(a) is rendered by transfer function set in (c). (b) The rendering image of a CT foot by using IS space (d), which can give more intuitive clues than the IGM space (see Fig. 12 in [7]).

3. Experiments and results

To evaluate the performance of the proposed method on the exploration of structures of interest, in this section, rendering results of various medical volume datasets [33] are compared which were generated with the proposed space and the IGM space. All of experiments were performed on a computer with a NVIDIA GeForce GT 630M graphics card, 2 GB RAM, Intel Core i3 2.20 GHz. The GPU ray caster was programmed with Cg shading language, the computations of the 3D SUSAN responses and the creation of IS space were implemented in CPU.

3.1. Blood vessels

An 8-bit aneurysm data ($256 \times 256 \times 256$) and a MR angiography volume data ($256 \times 320 \times 128$) were experimented for visualizing structures of blood vessels.

The aneurysm data was obtained by scanning the arteries of a human right half head. The IGM space shown in Fig. 2(b) was presented to six novice users and they were asked to select an area of interest. All of them indicated that these scatters were diffused the entire space in order that there was not a single shape to select. While the same six users were presented with the IS space (Fig. 2(a)), they now had a intuitive strip shape to choose, and all users selected the same shape mapping to the interesting features of the aneurysm data. As variations of the intensity values of the arteries, these scatters disperse seriously in the IGM space and there was not a single 'arch' shape (as shown in Fig. 2(b)). Thus the IGM space could not provide useful clues for users to understand the space and design appropriate transfer functions for the aneurysm data. And the exploration process would be a tedious trial-and-error task. Since scatters indicating blood vessel information were more compact and centralized (Fig. 2(a)), the IS space could provide users with intuitive clues in order that users just set a simple rectangular window on the 'trapezoid' clusters (Fig. 9(c)) and could get a sufficiently rendering result (Fig. 9(a)). As a result, the

exploration process of arteries with the IS space is more intuitive and easier than the IGM space.

The second volume data was a MRT Time-of-Flight angiography of a human head. Both the IGM space (Fig. 8(a)) and IS space (Fig. 8(b)) were used to identify the arterial blood vessels. Fig. 8(d) and Fig. 8(c) were their results, respectively. In the IS space, it was easier to design a transfer function, since the vessel structure had different SUSAN responses than other structures and was showed as a conspicuous structure (Fig. 8(b)). However, there was not a complete 'arch' shape for the vessel structure and the arch dispersed seriously in the IGM space (Fig. 8(a)). The rendering result of the proposed method contained more tiny blood vessels (blue window) and obtained more complete fine veins (yellow window) than that of the IGM space. Unlike the methods used in [2,34], even though radiologists are not familiar with these volume data and direct volume rendering, they can also obtain anatomical information of the whole cerebrovascular tree by just designing appropriate transfer functions. The proposed method which does not have to unintuitively operate on slices of 3D volume data [1,35], can obtain visualizations of anatomical segmentations by interacting with the IS transfer function space.

3.2. Bone structures

The first bone data was a CT hand ($492 \times 240 \times 155$), which was used by Svakhine et al. [36]. As shown in Fig. 3, unlike 3D video-fluoroscopy method [3,37], the proposed method need not to exploit segmentation procedure to reconstruct the 3D pose of objects. Compared with method used in [38], our method can get more complete bone structures. The proposed method could obtain 3D anatomical information of structures by just interacting with the 2D transfer function space. The same six novice users were presented with the IS space (Fig. 3(a)) and the IGM space (Fig. 3(c)) and were asked to determine the number of areas of interest. All of them said there were two features of interest. When asked to further select areas of interest by using rectangular windows, five users selected similar areas that would be interest to them and another user would be unsure of where to explore the space in the IS space. While all users indicated that they would be unsure of where to set the two rectangular windows in the IGM space, since arches spread seriously and arches belonging to different boundaries were intersected (yellow window in Fig. 3(c)). Thus it was almost impossible for users to simply select the bone structure in the IGM space. In the proposed space, it was much more easily and intuitive to select clusters because the scatters of boundary displayed as tightly 'trapezoid' shapes and there were a 'V' shape in the intersected 'trapezoid' shapes (yellow window in Fig. 3(a)). As shown in the yellow window of Fig. 3(b), the proposed method could show more details, such as the joints of the third and little fingers.

Then we explored a CT foot data ($256 \times 256 \times 256$) shown in Fig. 9. For the data contaminated seriously by noise, we increased intensity difference threshold to 20 in order to raise tolerance range about the maximum amount of noise. The noise in this data had little impact on the IS space (Fig. 9(d)), in which scatters were shown as a similar 'trapezoid' shape. It was easier for users to design a transfer function for discerning the bones than the IGM space (see Fig. 12 in [7]). Meanwhile, the proposed space (Fig. 9(b)) could discard some noise structures which appear in the IGM space.

3.3. Head

A MR head data ($256 \times 256 \times 99$) and a CT head data ($128 \times 256 \times 256$) were used to explore structures of interest.

The MR head data with skull partially removed to reveal brain was firstly experimented. The IGM space (Fig. 4(b)) was presented

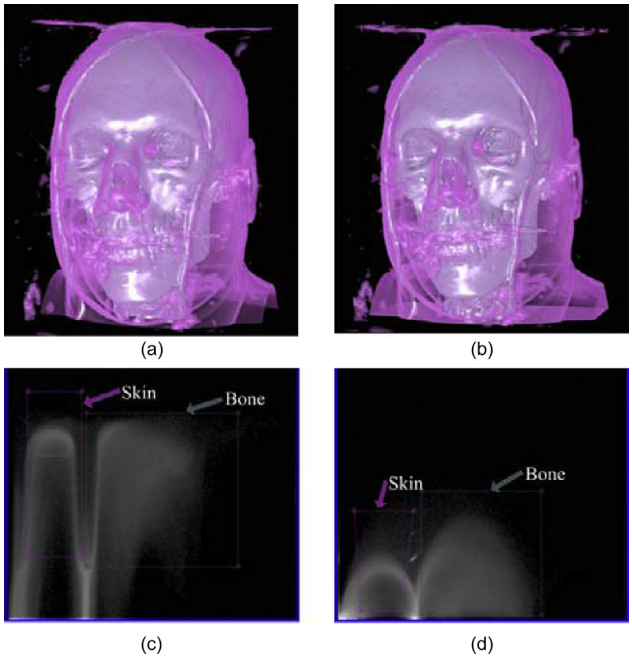

Fig. 10. Comparison of the IS space (c) with the IGM space (d) on a CT head data. Their rendering results are shown in (a) and (b), respectively.

to the same six novice users, who were asked to confirm how many areas of interest in the space. All users indicated that only one area of interest appears, since there was one 'arch' shape (yellow window in Fig. 4(b)). In fact, besides brain structure, skin structures are contained in the volume data. The same problem was asked for the IS space (Fig. 4(c)), four users said there were two areas of interest and two users were unsure of the number of areas of interest. In the IGM space, different 'arch' shapes which belonged to brain structure and skin structure were overlapped in order that they look like a single 'arch' shape (Fig. 4(b)), thus it is impossible for users to distinguish these arches and design transfer functions. And users may lose some tissues of interest just using the IGM space. While the proposed method could provide meaningful suggestions for users to correctly identify these overlapped arches and obtain desired images (Fig. 4(a)).

Another data was a CT head of visible male ($128 \times 256 \times 256$). There was not a single 'arch' shape in the IGM space (Fig. 10(d)), which resulted from transforms of intensities of the same materials. This made it more difficult to set proper transfer functions and implemented fine adjustments about them, because arches spread seriously and were mostly near to each other. To get a satisfying result (Fig. 10(b)), the process of transfer function design would be a time-consuming trial-and-error task. In comparison, skin and bone structures could be easily identified in the IS space (Fig. 10(c)), since these boundaries information were prominently displayed as 'trapezoid' shapes and more tightly clustered. By setting simple rectangular windows to enwrap the salient regions (Fig. 10(c)), users could gain a satisfying result (Fig. 10(a)), which need little fine adjustment operations. Unlike method used in [38], our method can not only need not interact with 2D slices of 3D volume data, but also obtain more complete head structures. Furthermore, by rendering shin structures, we can get more anatomical information.

3.4. Tissue structures

The ability of the proposed method to distinguish different materials could be used for many purposes. A common work was to explore the ventricles in a MRI scan of the head ($256 \times 256 \times 124$).

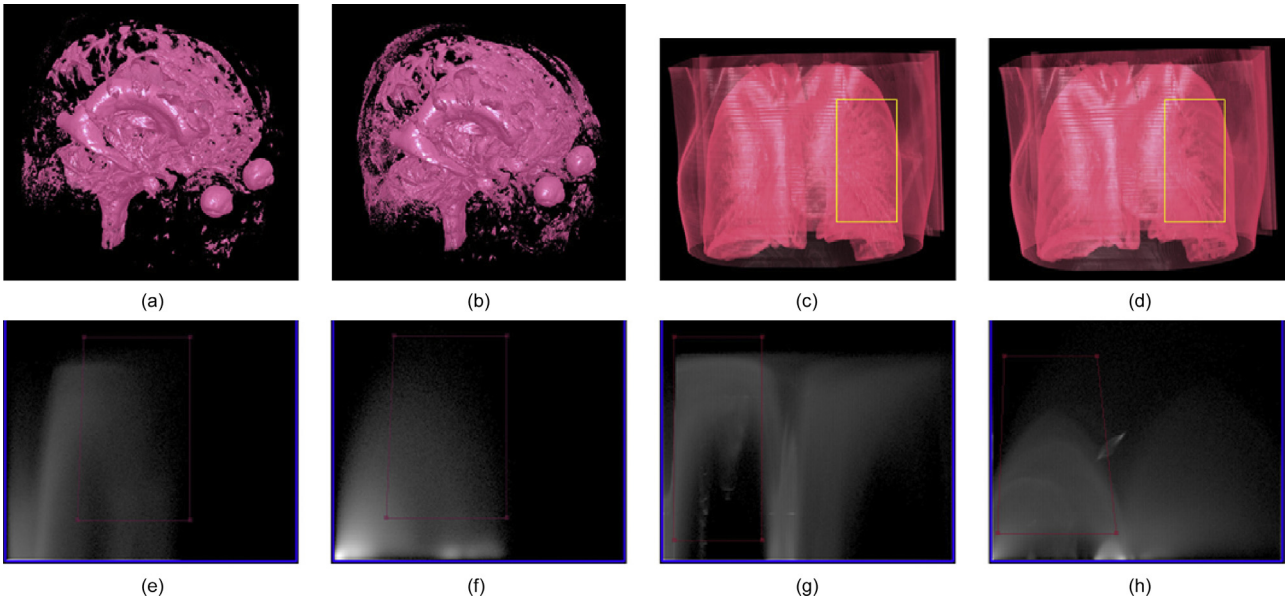

Fig. 11. Two experiments for comparing the identify capability of the IS space and the IGM space on different tissue structures: a MRI ventricle (two left columns) and CT chest (two right columns). Boundary information of different materials are shown as 'trapezoid' shapes in the IS space ((e) and (g)), it is more intuitive to design transfer functions than the IGM space ((f) and (h)). Rendering images are shown on top of their transfer function space. The proposed method (yellow window in (c)) obtains more bronchioles than the IGM space (yellow window in (d)). (For interpretation of the references to color in this figure legend, the reader is referred to the web version of the article.)

Different results of this task for different transfer function spaces were shown in the left two columns of Fig. 11. With the IGM space (Fig. 11(f)), the ventricles could not be correctly identified because many uninterested tissues appear in the rendering image (Fig. 11(b)). In addition, it was hard to set and refine transfer functions in the IGM space because these scatters were not shown as a single 'arch' shape and they diffused seriously. In comparison, the proposed method could clearly distinguish the ventricles and discard some uninterested tissues as shown in Fig. 11(a). It could be seen that boundary information of the ventricles were shown as a compact 'trapezoid' shape (Fig. 11(e)), which made it much easier to design a transfer function.

Another work was detection of lungs in a CT chest ($384 \times 384 \times 240$). As shown in Fig. 11(h), it was not easily for users to understand boundary information in the IGM space and define transfer functions, since 'arch' of the same boundary dispersed seriously and adjacent arches were intersected. In comparison, 'trapezoid' shapes were compact and distinguishable in the IS space (Fig. 11(g)), which provided more intuitive clues for users to distinguish boundary information. Thus users could easily design transfer functions just using a simple quadrilateral widget to obtain a desired images. Furthermore, the proposed method (yellow window in Fig. 11(c)) obtained more bronchioles than the IGM space (yellow window in Fig. 11(d)). Unlike method used in [24,35], the proposed method can obtain more real visualization of a chest and more detailed information.

4. Conclusion

A novel 2D IS transfer function space have been proposed by combining the intensity with 3D SUSAN edge response of the volume data. With the new space, users are able to better separate different materials and more easily understand the space to design transfer functions than the IGM space. To obtain visualizations of anatomical structures, unlike unintuitive and tedious methods operating on slices of 3D volume data, our method just need understand boundary information in the transfer function space and then design transfer functions by interacting with the space. Even for noisy data, boundary information of different materials can be still distinguished and displayed as similar 'trapezoid' shapes in the space. Thus it can provide much more intuitive suggestions for users to design appropriate transfer functions and visualize structures of interest than the IGM space in realistic volume data. From our experiments, it is clear that the boundary information in the proposed space can be more easily identified than the IGM space. Thus users can design transfer functions by directly setting quadrilateral widgets in the IS space and need little adjustment operations. This is particularly useful for radiologists who have not much experience about designing transfer functions. Also, the rendering results with the proposed method can contain more details of anatomical structures.

Acknowledgement

This research is partly supported by NSFC, China (No: 61375048) and 973 Plan, China (No. 2015CB856004).

References

[1] T. Heinone, P. Dastidar, P. Kauppinen, J. Malmivuo, H. Eskola, Semi-automatic tool for segmentation and volumetric analysis of medical images, Med. Biol. Eng. Comput. 36 (3) (1998) 291–296.
[2] B. Liu, F. Zhou, X. Bai, Improved c-arm cardiac cone beam CT based on alternate reconstruction and segmentation, Biomed. Signal Process. Control 13 (2014) 113–122.
[3] S.A. Banks, W.A. Hodge, Accurate measurement of three-dimensional knee replacement kinematics using single-plane fluoroscopy, IEEE Trans. Biomed. Eng. 43 (6) (1996) 638–649.
[4] W.E. Lorensen, H.E. Cline, Marching cubes: a high resolution 3D surface construction algorithm, SIGGRAPH Comput. Graph. 21 (4) (1987) 163–169.
[5] M. Levoy, Display of surfaces from volume data, IEEE Comput. Graph. Appl. 8 (3) (1988) 29–37.
[6] J. Kniss, G. Kindlmann, C. Hansen, Multidimensional transfer functions for interactive volume rendering, IEEE Trans. Vis. Comput. Graph. 8 (3) (2002) 270–285.
[7] R. Maciejewski, Y. Jang, I. Woo, H. Jänicke, K. Gaither, D. Ebert, Abstracting attribute space for transfer function exploration and design, IEEE Trans. Vis. Comput. Graph. 19 (1) (2013) 94–107.
[8] S. Stegmaier, M. Strengert, T. Klein, T. Ertl, A simple and flexible volume rendering framework for graphics-hardware-based raycasting, in: Fourth International Workshop on Volume Graphics, 2005, pp. 187–241.

[9] C.P. Botha, F.H. Post, New technique for transfer function specification in direct volume rendering using real-time visual feedback, in: Medical Imaging 2002 Visualization, Image-Guided Procedures and Display, Vol. 4681, SPIE, 2002, pp. 349–356.
[10] G. Kindlmann, J. Durkin, Semi-automatic generation of transfer functions for direct volume rendering, in: Proceedings of the 1998 IEEE Symposium on Volume Visualization, 1998, pp. 79–86.
[11] M. Chen, H. Jänicke, An information-theoretic framework for visualization, IEEE Trans. Vis. Comput. Graph. 16 (6) (2010) 1206–1215.
[12] S. Roettger, M. Bauer, M. Stamminger, Spatialized transfer functions, in: Proceedings Eurographics/IEEE-VGTC Symposium on Visualization, 2005, pp. 271–278.
[13] Y. Wang, J. Chen, W. Zhang, T. Dong, G. Shan, X. Chi, Efficient volume exploration using the Gaussian mixture model, IEEE Trans. Vis. Comput. Graph. 17 (11) (2011) 1560–1573.
[14] J. Marks, B. Andalman, P. Beardsley, H. Pfister, et al., Design galleries: a general approach to setting parameters for computer graphics and animation, in: Proceedings of the ACM SIGGRAPH Conference on Computer Graphics, ACM, 1997, pp. 389–400.
[15] S. Park, C. Bajaj, Feature selection of 3D volume data through multidimensional transfer functions, Pattern Recognit. Lett. 28 (3) (2007) 367–374.
[16] I.W.O. Serlie, F.M. Vos, R. Truyen, F.H. Post, L.J. van Vliet, Classifying CT image data into material fractions by a scale and rotation invariant edge model, IEEE Trans. Image Process. 16 (12) (2007) 2891–2904.
[17] C. Correa, K. Ma, Size-based transfer functions: A new volume exploration technique, IEEE Trans. Vis. Comput. Graph. 14 (6) (2008) 1380–1387.
[18] S. Wesarg, M. Kirschner, M.F. Khan, 2D histogram based volume visualization: combining intensity and size of anatomical structures, Int. J. Comput. Assist. Radiol. Surg. 5 (6) (2010) 655–666.
[19] S. Marchesin, J.-M. Dischler, C. Mongenet, Per-pixel opacity modulation for feature enhancement in volume rendering, IEEE Trans. Vis. Comput. Graph. 16 (4) (2010) 560–570.
[20] Y. Wu, H. Qu, Interactive transfer function design based on editing direct volume rendered images, IEEE Trans. Vis. Comput. Graph. 13 (5) (2007) 1027–1040.
[21] M. Chan, Y. Wu, W. Mak, W. Chen, H. Qu, Perception-based transparency optimization for direct volume rendering, IEEE Trans. Vis. Comput. Graph. 15 (6) (2009) 1283–1290.
[22] M. Ruiz, A. Bardera, I. Boada, I. Viola, M. Feixas, M. Sbert, Automatic transfer functions based on informational divergence, IEEE Trans. Vis. Comput. Graph. 17 (12) (2011) 1932–1941.
[23] C. Correa, K. Ma, Visibility histograms and visibility-driven transfer functions, IEEE Trans. Vis. Comput. Graph. 17 (2) (2011) 192–204.
[24] R. Liang, Y. Wu, F. Dong, G. Clapworthy, Accumulation of local maximum intensity for feature enhanced volume rendering, Vis. Comput. 28 (6–8) (2012) 625–633.
[25] C. Correa, K. Ma, The occlusion spectrum for volume classification and visualization, IEEE Trans. Vis. Comput. Graph. 15 (6) (2009) 1465–1472.
[26] I. Viola, A. Kanitsar, M.E. Gröller, Importance-driven feature enhancement in volume visualization, IEEE Trans. Vis. Comput. Graph. 11 (4) (2005) 408–418.
[27] J.-S. Praßni, T. Ropinski, J. Mensmann, K. Hinrichs, Shape-based transfer functions for volume visualization, in: IEEE Pacific Visualization Symposium 2010, IEEE Computer Society, 2010, pp. 9–16.
[28] S.M. Smith, J.M. Brady, SUSAN – a new approach to low level image processing, Int. J. Comput. Vis. 23 (1) (1997) 45–78.
[29] B. Marusic, P. Skocir, J. Tasic, A. Kosir, Application of the SUSAN filter to wavelet video-coding artifact removal, AEU Int. J. Electron. Commun. 60 (1) (2006) 56–64.
[30] Z. Mao, L. Ma, M. Zhao, X. Xiao, SUSAN structure preserving filtering for mesh denoising, Vis. Comput. 22 (4) (2006) 276–284.
[31] C. Claus, R. Huitl, J. Rausch, W. Stechele, Optimizing the SUSAN corner detection algorithm for a high speed FPGA implementation, in: International Conference on Field Programmable Logic and Applications, 2009, 2009, pp. 138–145.
[32] J. Yu, J.Y.W. Tan, Ultrasound speckle reduction by a SUSAN-controlled anisotropic diffusion method, Pattern Recognit. 43 (9) (2010) 3083–3092.
[33] The Volume Library, Available at: http://lgdv.cs.fau.de/External/vollib/
[34] J. Hao, M. Li, F. Tang, Adaptive segmentation of cerebrovascular tree in time-of-flight magnetic resonance angiography, Med. Biol. Eng. Comput. 46 (1) (2008) 75–83.
[35] S. Zhou, Y. Cheng, S. Tamura, Automated lung segmentation and smoothing techniques for inclusion of juxtapleural nodules and pulmonary vessels on chest CT images, Biomed. Signal Process. Control 13 (2014) 62–70.
[36] N.A. Svakhine, D.S. Ebert, W.M. Andrews, Illustration-inspired depth enhanced volumetric medical visualization, IEEE Trans. Vis. Comput. Graph. 15 (1) (2009) 77–86.
[37] G. Tarroni, L. Tersi, C. Corsi, R. Stagni, Prosthetic component segmentation with blur compensation: a fast method for 3D fluoroscopy, Med. Biol. Eng. Comput. 50 (6) (2012) 631–640.
[38] R. Liang, Z. Pan, M. Krokos, M. Chen, J. Bao, C. Li, Fast hardware-accelerated volume rendering of CT scans, J. Disp. Technol. 4 (4) (2008) 431–436.